AUT Journal of Electrical Engineering

AUT J. Elec. Eng., 54(1) (2022) 29-38
DOI: 10.22060/eej.2021.18885.5363

The New Generation of Attitude Determination Sensor for LEO Satellite based on Induced Electric Field

Mohsen Rezaei[1,2], Kamran Raissi[1*], Hamed Hashemi Mehne[2], Yaser Norouzi[3]

[1] Department of Aerospace, Amirkabir University of Technology, Tehran, Iran

[2] Aerospace Research Institute, Tehran, Iran

[3] Department of Electrical Engineering, Amirkabir University of Technology, Tehran, Iran

ABSTRACT: Many satellites use closed-loop attitude control to carry out their missions. They use several sensors such as sun, magnetometer, and star tracker to close the control loop. Sun sensors are not operational during the eclipse and therefore, one of the observed vectors is lost. For this reason, attitude determination in eclipse can be a challenging issue for control engineers. This paper presents a novel idea for producing a new generation of sensors that can measure the induced electric field vector not only in eclipse, but also in all orbit. This electric field comes from a high velocity of the spacecraft in the magnetic field of the Earth. This vector is always perpendicular to the magnetic field; thus, it is never aligned with the magnetic vector and never causes singularity and accuracy decrease. The induced electric field is measured by three RC circuits that are actuated by sinusoidal voltage. The dielectrics of the capacitors are made of ferroelectric materials; therefore, the induced voltage affects the permittivity and voltage of the capacitor. By measuring and calibrating this effect in three perpendicular axes, we can measure the three components of the electric field vector. The theory of the proposed sensor has been developed, and simulation studies validate the results.

Review History:

Received: Aug. 23, 2020
Revised: Jul. 14, 2021
Accepted: Sep. 11, 2021
Available Online: Jun. 01, 2022

Keywords:

Attitude determination
MEMS sensors
capacitive sensors
nonlinear capacitors
ferroelectric

1- Introduction

The number of LEO[1] satellites is growing day by day, and their applications improve drastically. Decreasing cost, weight, size, and increasing the accuracy and performance are significant issues. The new generation of sensors and actuators can help to produce a new generation of satellites with low cost and weight, high accuracy, and better performance. However, there is a long way to producing a new generation of the proposed sensor, yet the present investigation offers a novel approach to achieve this goal.

Most spacecrafts fulfill their mission by controlling their attitude relative to the desired reference frame in orbit. Usually, closed-loop control is applied to this task. The attitude determination provides feedback for the control system. The main approaches for determining the attitude of the spacecraft are deterministic and recursive methods [1-3].

At least two types of sensors are needed to measure two known vectors in the body frame for the deterministic approach. These vectors must not be parallel. The sun sensor is one of the most useful sensors to provide one of these vectors, but it isn't useable during an eclipse. The field of view limitation is another disadvantage of sun sensors, which forces the designer to use several sun sensors to cover the whole view [2-3].

The magnetometer is another useful sensor, widely used by the designer to provide the second vector for attitude determination. This sensor measures the magnetic field vector in the satellite's body frame to use in the attitude determination algorithm. There are many mechanisms for measuring magnetic fields, such as: microelectromechanical system resonator based sensor [4-9], AMR[2] [9], and Fluxgate [9].

Star tracker can measure several vectors by itself and calculate the attitude of spacecraft with respect to a reference frame. However, these sensors have several disadvantages such as heavyweight, high power consumption, and cost.

The idea of measuring another type of vector is proposed by Rezaei et al. [10]. The authors have introduced the new sensor, which can measure the Lorentz force as a known vector in the body and reference frame to determine the spacecraft's attitude. This vector can be used instead of or with the sun vector. The above mentioned Lorentz force is created by high linear velocity of the satellite and Earth magnetic field.

In this paper, we propose another way for measuring the induced electric field using three RC circuits [3] with specific capacitors. The dielectric of the capacitors is made

1 Low Earth Orbit

2 Anisotropic magneto-resistive

3 resistor–capacitor circuit

*Corresponding author's email: k_raissi@aut.ac.ir

of ferroelectric material and has nonlinear permittivity [11].

In the following sections, we first introduce one of the attitude determination methods, which helps the reader to better understand the proposed sensor performance. The theory and mathematical model of the sensor are described. In section 4, the simulation studies are performed, and finally, the conclusions are presented in section 5.

2- Attitude Determination Methods

At least two unparalleled vectors are needed to determine the spacecraft's attitude, and these vectors must be known in both body and reference frames. The vectors are usually measured in the body frame of a spacecraft by two different sensors, and the components of these vectors in the reference frame are obtained using mathematical models.

There are two main approaches to the attitude determination of a spacecraft, deterministic and recursive estimation. In deterministic methods, which are based on linear algebra, we minimize a loss function proposed by Wahba [12] to determine the attitude of a spacecraft with respect to the reference frame. The methods such as the Q-method, QUEST[1], OTOQUEST[12], and Triad are deterministic. On the other hand, the recursive algorithms use the governing dynamics, previous and current state of the system to estimate the unobservable state. In case of data missing for a while, the state is predictable. However, the estimation error would increase if a portion or all the data is unavailable for a long time. The Kalman Filter and Extended Kalman Filter (EKF) are recursive methods [14].

To understand proposed sensor's performance, we first describe the Triad algorithm. In this approach, a transformation matrix between the spacecraft body frame and the reference frame is found, and the attitude of the spacecraft relative to the reference frame is obtained. Primarily, an intermediate frame "A" is defined by three orthogonal unit vectors; $\hat{a}_1$, $\hat{a}_2$, and $\hat{a}_3$, which are known relative to the body and the reference frames. Afterwards, the intermediate frame is omitted, and the attitude of the body frame is found relative to the reference frame. At least two kinds of sensors (i.e. magnetometer ($\vec{B}_{earth}$) and proposed sensor ($\vec{E}_{ext}$)), are required to provide the known frame relative to the body frame according to the following equations:

$$\text{Let, } \hat{a}_1 = \frac{\vec{E}_{ext}}{\left|\vec{E}_{ext}\right|} = \hat{e} \quad \text{thus:} \tag{1}$$

$$\hat{a}_{1b} = \hat{e}_b$$

"$\hat{e}_b$" is the unit induced electric field in the body frame, which is measured by the proposed sensor. This vector must be known in reference frame in advance. The induced electric field unit vector "$\hat{e}_r$" is calculated using Earth Magnetic Field's mathematical model and information of the spacecraft's position in the reference frame. Therefore, $\hat{a}_{1r}$ is the first unit vector of the intermediate frame and equal to

$$\hat{a}_{1r} = \hat{e}_r \tag{2}$$

$\hat{a}_{1b}$ and $\hat{a}_{1r}$ are the first unit vectors of the intermediate frame, which are defined in body and reference frame, respectively. The second vectors of the intermediate frame are perpendicular to the first one are:

$$\hat{a}_{2b} = \frac{\hat{e}_b \times \hat{b}_b}{\left|\hat{e}_b \times \hat{b}_b\right|},\ \hat{a}_{2r} = \frac{\hat{e}_r \times \hat{b}_r}{\left|\hat{e}_r \times \hat{b}_r\right|} \tag{3}$$

Where "x" is the cross product. $\hat{b}_b$ is the unit vector of the Earth Magnetic Field in the body frame, which is measured by the magnetometer and considered as the second type of sensor. The $\hat{b}_r$ is the Earth Magnetic Field defined in the reference frame. It is calculated by knowing the spacecraft's position and the mathematical model of the Earth Magnetic Field. The third unit vector is found by the following equations:

$$\hat{a}_{3b} = \frac{\hat{a}_{1b} \times \hat{a}_{2b}}{\left|\hat{a}_{1b} \times \hat{a}_{2b}\right|},\ \hat{a}_{3r} = \frac{\hat{a}_{1r} \times \hat{a}_{2r}}{\left|\hat{a}_{1r} \times \hat{a}_{2r}\right|} \tag{4}$$

Therefore, using $\hat{a}_1$, $\hat{a}_2$, and $\hat{a}_3$, the intermediate frame is obtained by:

$$R^{ba} = \begin{bmatrix} \hat{a}_{1b} & \hat{a}_{2b} & \hat{a}_{3b} \end{bmatrix} \tag{5}$$

Thus, R^{ba} is the transformation matrix between the body frame "B" and the intermediate frame "A," and:

$$R^{ra} = \begin{bmatrix} \hat{a}_{1r} & \hat{a}_{2r} & \hat{a}_{3r} \end{bmatrix} \tag{6}$$

is the transformation matrix between the reference frame and the intermediate frame. Finally, the transformation matrix between the body frame and the reference frame is:

$$R^{br} = R^{ba} R^{ar} = \begin{bmatrix} \hat{a}_{1b} & \hat{a}_{2b} & \hat{a}_{3b} \end{bmatrix} \begin{bmatrix} \hat{a}_{1r} & \hat{a}_{2r} & \hat{a}_{3r} \end{bmatrix}^T \tag{7}$$

1 QUaternion ESTimator

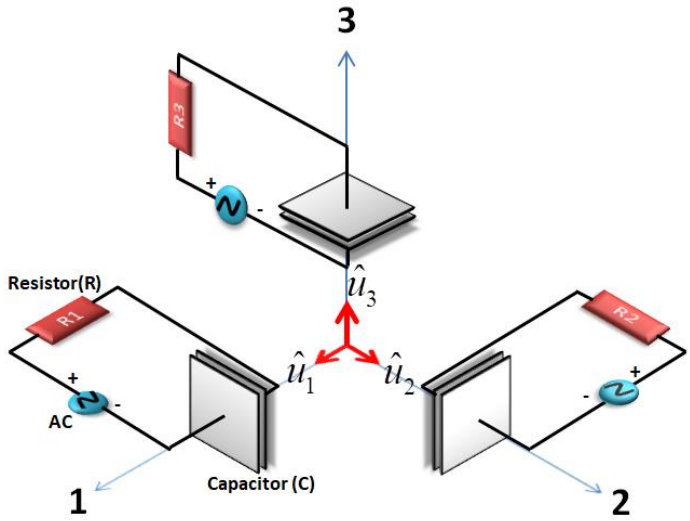

Fig. 1. Schematic diagram of the three orthogonal RC circuits.

where determines the attitude of the body frame with respect to the reference frame.

3- The Theory and Mathematical Model of Proposed Sensor

In this section, we present the theory and mathematical model of proposed sensor. As mentioned earlier, the sensor is composed of three RC circuits that are mounted in three orthogonal axes. The dielectrics of capacitors are made of ferroelectric material with nonlinear permittivity, which changes under the influence of the applied external electric field (E). Johnson [15] has obtained the following function that describes the variation of dielectric constant for the external electric field:

$$\varepsilon(E) = \frac{\varepsilon(0)}{\left[1 + \alpha\varepsilon^3(0)E^2\right]^{1/3}} \tag{8}$$

where $\varepsilon(0)$ is the relative permittivity at zero field, and α is a positive constant. The capacitor of each RC circuit is excited by sinusoidal voltage. $V_C(t)$ and $E_C(t)$ are the voltage of the capacitor and the magnitude of the electric field between the plates of the capacitors, respectively.

$$\begin{aligned} V_C(t) &= V_m \sin(\omega t) \\ E_C(t) &= \frac{V_C}{d} = E_m \sin(\omega t) \end{aligned} \tag{9}$$

where d and ω are the distance and alternating voltage frequency of the plates, respectively. When the capacitors move with high velocity in the magnetic field, the external electric field $\vec{E}_{exi}$ is applied to the dielectric of each capacitor. Therefore:

$$\vec{E}_{ext} = \vec{V}_{sat} \times \vec{B}_{earth} \tag{10}$$

where $\vec{V}_{sat}$ and $\vec{B}_{earth}$ are the satellite's velocity and the Earth magnetic field in the position of the spacecraft. We can define the external applied electric field in body frame by:

$$\vec{E}_{ext} = E_{ext1}\hat{u}_1 + E_{ext2}\hat{u}_2 + E_{ext3}\hat{u}_3 \tag{11}$$

$\hat{u}_i$, $i = 1,2,3$ are the unit vectors in three orthogonal directions of the satellite's body frame, and each capacitor is mounted along one of them (Figure 1). Thus, the summation of the electric field in direction $i = 1,2,3$ is:

$$E_{\sum i} = E_C + E_{ext\,i} \tag{12}$$

The current i in the RC circuit is:

$$\left.\begin{aligned} i &= \frac{dq}{dt} \\ q &= CV_C = CV_m \sin(\omega t) \end{aligned}\right\} \Rightarrow i = \frac{d(CV_C)}{dt} = \frac{dC}{dt}V_C + C\frac{dV_C}{dt} \tag{13}$$

Where C and q are the capacitance and the charge on the plates of the capacitor, respectively. Since the dielectrics of the capacitors are made of a ferroelectric material, the capacitance changes by the applied external electric field.

Thus:

$$C = \varepsilon_0 \varepsilon(E_\Sigma)\frac{A}{d} \Rightarrow \frac{dC}{dt} = \frac{d\varepsilon(E_\Sigma)}{dt}\frac{\varepsilon_0 A}{d} = \frac{d\varepsilon(E_\Sigma)}{dE_\Sigma}\frac{dE_\Sigma}{dt}\frac{\varepsilon_0 A}{d} \quad (14)$$

Where A and ε_0 are the area of each plates of the capacitor and the permittivity of vacuum[1], respectively. According to Johnson's function (8):

$$C = \varepsilon_0 \varepsilon(E_\Sigma)\frac{A}{d} \Rightarrow \frac{dC}{dt} = \frac{d\varepsilon(E_\Sigma)}{dt}\frac{\varepsilon_0 A}{d} = \frac{d\varepsilon(E_\Sigma)}{dE_\Sigma}\frac{dE_\Sigma}{dt}\frac{\varepsilon_0 A}{d} \quad (15)$$

Considering equations (9), (12), (14), and (15), and assuming the frequency of variation of $\vec{V}_{sat}$ and $\vec{B}_{earth}$ are much less than ω; therefore:

$$\frac{dC}{dt} = -\frac{2}{3}\frac{a\varepsilon^4(0)E_\Sigma(t)}{\left(1+a\varepsilon^3(0)E_\Sigma^2(t)\right)^{4/3}} \cdot \frac{V_m \omega \varepsilon_0 A}{d^2}\cos(\omega t) \quad (16)$$

According to (13):

$$i = -\frac{2}{3}\frac{a\varepsilon^4(0)E_\Sigma(t)}{\left(1+a\varepsilon^3(0)E_\Sigma^2(t)\right)^{4/3}} \cdot V_m \omega\cos(\omega t)\frac{\varepsilon_0 A}{d^2}(V_m \sin(\omega t)) + \varepsilon(E_\Sigma)\frac{\varepsilon_0 A}{d}V_m \omega\cos(\omega t) \quad (17)$$

Now by using equation (8), (9), and (12):

$$i = -\frac{2}{3}\frac{a\varepsilon^4(0)V_m^2 \omega\frac{\varepsilon_0 A}{d^2}}{\left(1+a\varepsilon^3(0)\left\{E_{ext}+E_m\sin(\omega t)\right\}^2\right)^{4/3}} \times \left\{E_{ext}+E_m\sin(\omega t)\right\}\cos(\omega t)\sin(\omega t)) + \left[\frac{\varepsilon(0)}{1+a\varepsilon(0)^3\left\{E_{ext}+E_m\sin(\omega t)\right\}^2}\right]^{1/3}\frac{\varepsilon_0 A}{d}V_m \omega\cos(\omega t) \quad (18)$$

let,

$$\lambda = -\frac{1}{3}\frac{a\varepsilon^2(0)}{\left(1+a\varepsilon^3(0)E_\Sigma^2(t)\right)^{4/3}} \quad (19)$$

Thus,

$$i = \lambda V_m^2 \frac{\varepsilon_0 A}{d^2}E_\Sigma \omega\sin(2\omega t) + \varepsilon(E_\Sigma)\frac{\varepsilon_0 A}{d}V_m \omega\cos(\omega t) \quad (20)$$

According to (9) and (12), the equation (20) can be written as follows:

$$i = \lambda V_m^2 \frac{\varepsilon_0 A}{d^2}\omega\left(E_{ext}+E_m\sin(\omega t)\right)\sin(2\omega t) + \varepsilon(E_\Sigma)\frac{\varepsilon_0 A}{d}V_m \omega\cos(\omega t) = \lambda V_m^2 \frac{\varepsilon_0 A}{d^2}\omega E_{ext}\sin(2\omega t) + \lambda V_m^2 \frac{\varepsilon_0 A}{d^2}\omega E_m \sin(\omega t)\sin(2\omega t) + \varepsilon(E_\Sigma)\frac{\varepsilon_0 A}{d}V_m \omega\cos(\omega t) \quad (21)$$

Therefore:

$$i = \lambda V_m^2 \frac{\varepsilon_0 A}{d^2}\omega E_{ext}\sin(2\omega t) + \frac{\lambda}{2}V_m^2 \frac{\varepsilon_0 A}{d^2}\omega E_m\{\cos(\omega t) - \cos(3\omega t)\} + \varepsilon(E_\Sigma)\frac{\varepsilon_0 A}{d}V_m \omega\cos(\omega t) \quad (22)$$

Finally, the equation (22) can be simplified as follows:

$$i = \left\{\frac{\lambda}{2}V_m^2 \frac{\varepsilon_0 A}{d^2}\omega E_m + \varepsilon(E_\Sigma)\frac{\varepsilon_0 A}{d}V_m \omega\right\}\cos(\omega t) + \lambda V_m^2 \frac{\varepsilon_0 A}{d^2}\omega E_{ext}\sin(2\omega t) - \frac{\lambda}{2}V_m^2 \frac{\varepsilon_0 A}{d^2}\omega E_m \cos(3\omega t) \quad (23)$$

If E_m is sufficiently small, then λ in (19) can be considered as a constant:

$$\lambda \approx -\frac{1}{3}a\varepsilon^2(0) \quad (24)$$

1

Table 1. Simulation Parameters.

Symbol	Quantity	Value	Unit
$\varepsilon(0)$	Relative permittivity at zero field	1000	-
α	Positive constant	5.479E-19	cm^2/V^2
A	Area of capacitor's plates	0.01	m^2
d	The gap between the capacitor's plates	1e-2	M
V_m	The peak capacitor's voltage	5	V
ω	The voltage alternating angular frequency	2000π	Hz

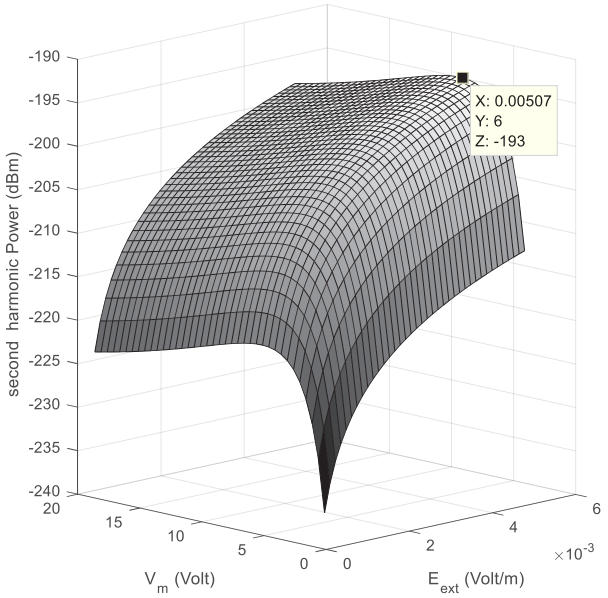

Fig. 2. the variation of the second harmonic amplitude for the current signal in different E_{ext} and V_m .

From equation (23), the second harmonic amplitude is proportional to the component of the external electric field (E_{ext}). Therefore, by measuring and calibrating the second harmonic amplitude of the current signal of each circuit, we can compute the components of the external electric field vector. Concerning the expressions given in section 2, this vector could be used in different algorithms to determine a spacecraft's attitude. In the following section, we will explain the effect of the external electric field on the current of each RC circuit with simulation studies.

4- Simulation Studies

For the following simulation studies the major parameters are given in table 1.

The $\varepsilon(0)$ and α have been chosen for lead lanthanum zirconate titanate (PLZT) [16] .

The current of each circuit is calculated by using equation (25):

$$i = \frac{q(t+\Delta t) - q(t)}{\Delta t} \tag{25}$$

The amplitude of the second harmonic of current signal is calculated for different E_{ext} , and V_m is shown in figure 2. It is clear that the second harmonic amplitude at each V_m increases as E_{ext} also increases, and has a direct relation with E_{ext} . On the other hand, the rate of second harmonic amplitude variation with respect to different V_m s indicates

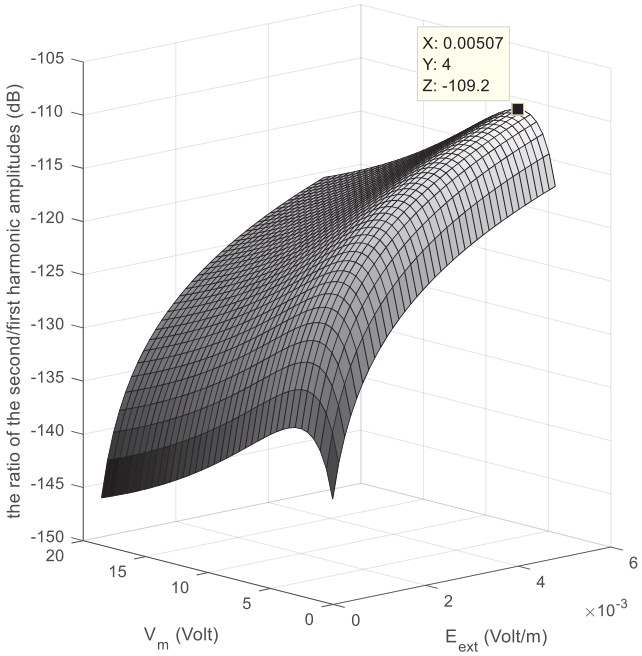

Fig. 3. the ratio of the second harmonic to the first harmonic amplitudes of the signal in different E_ext and V_m.

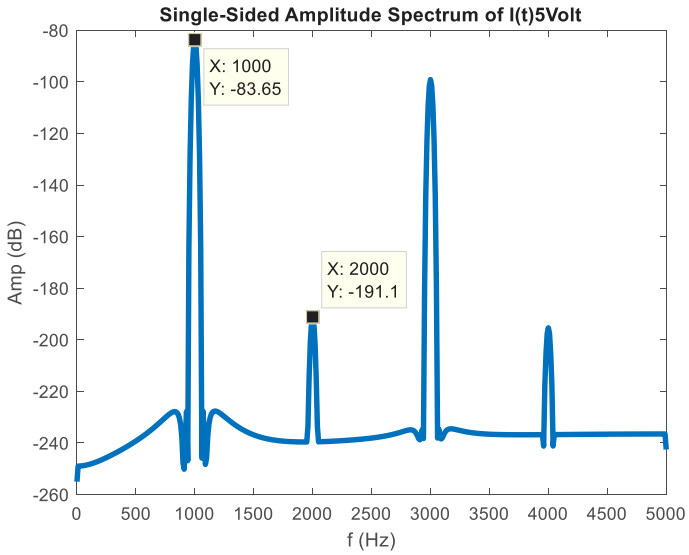

Fig. 4. The FFT plot of the current signal ($E_{ext} = 0.0065(V/m)$)

that the maximum of the second harmonic amplitude has occurred at $V_m = 5volts$. Therefore, for the parameters proposed in table 1, $V_m = 5volts$ could be considered as a suitable amplitude for sinusoidal voltage exciting.

Figure 3 depicts the ratio of the second harmonic to the first harmonic amplitudes of the signal in different E_{ext} and V_m .

As mentioned earlier, we expect that there is a relationship between second harmonic amplitude and E_{ext} . To justify this matter, the fast Fourier transform of the RC circuit current signal for different E_{ext} were obtained. Figure (4) is a sample of these plots when $E_{ext} = 0.0065(V/m)$.

Figure 5 shows the relatively linear behavior of the second harmonic amplitude variation with respect to E_{ext} , which approves our analytical results in previous sections.

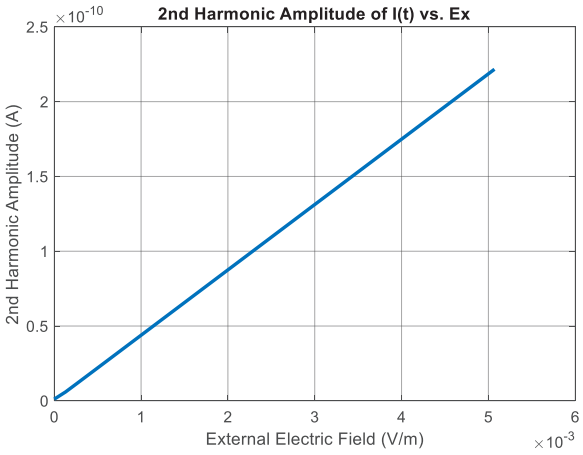

Fig. 5. The second harmonic amplitude vs. external electric field E_{ext}

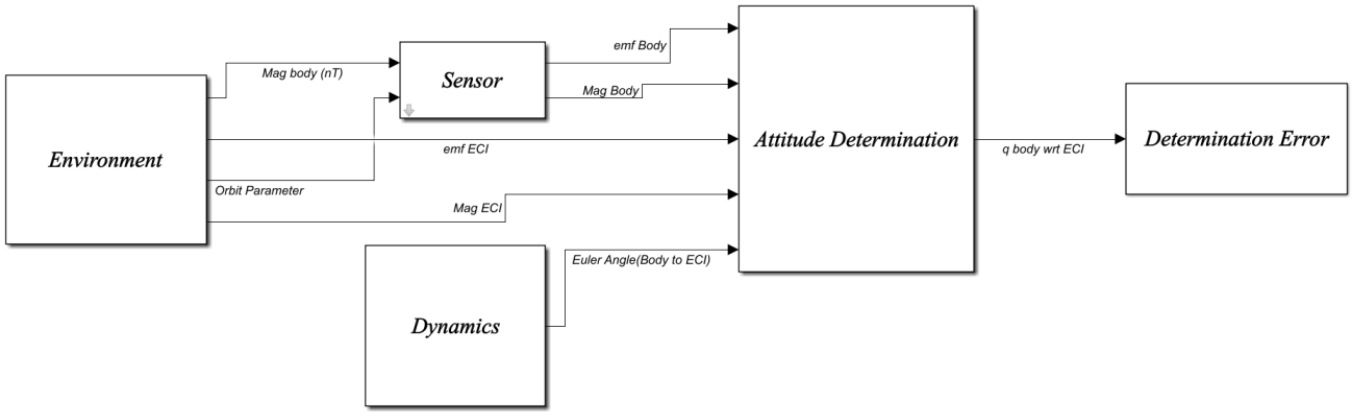

Fig. 6. The simulation of satellite in a low earth orbit (LEO) in MATLAB SIMULINK

5- The Effect of the Solar Storm

A satellite's attitude determination accuracy is affected by several phenomena, such as the error of position estimation, deviation in the geomagnetic model, temperature, etc. For instance, in this part the effect of the solar storm is investigated. According to [17], the solar storm has been modeled as a Gaussian noise with a standard deviation equal to 100 nT in each axis. The position of the satellite in orbit is modeled and propagated over the simulation time. The vector of the magnetic model of the Earth and the solar vector are calculated in the position of the satellite in the inertial reference frame. The simulation is made in MATLAB SIMULINK according to figure 6.

The effect of a solar storm on the attitude determination by the proposed sensor is shown in figure 7. The Euler angles errors are σ_ϕ= 0.5648 deg, σ_θ=0.5457 deg, and σ_ψ=0.6378 deg. They are the standard deviations of each Euler angle error without using EKF[1].

Kalman filter and data fusion of different sensors can be used to reduce the effect of solar storms on satellite attitude determination errors. In this investigation, data of the proposed sensor has been used alongside the data of magnetometer and gyroscope to reduce the effect of solar storms. The Euler angles error has been shown in figure 8. The standard deviations of each Euler angle error are as follows: σ_ϕ= 0.1951 deg, σ_θ= 0.1760 deg, and σ_ψ= 0.1809 deg. The results have been improved by using EKF and fusing the data of the magnetometer and gyroscope.

The effect of a solar storm on the proposed sensor is not drastic on the error of attitude determination, but also it can decrease by using filtering and estimation algorithms and fusing the data of other sensors.

1 Extended Kalman Filter

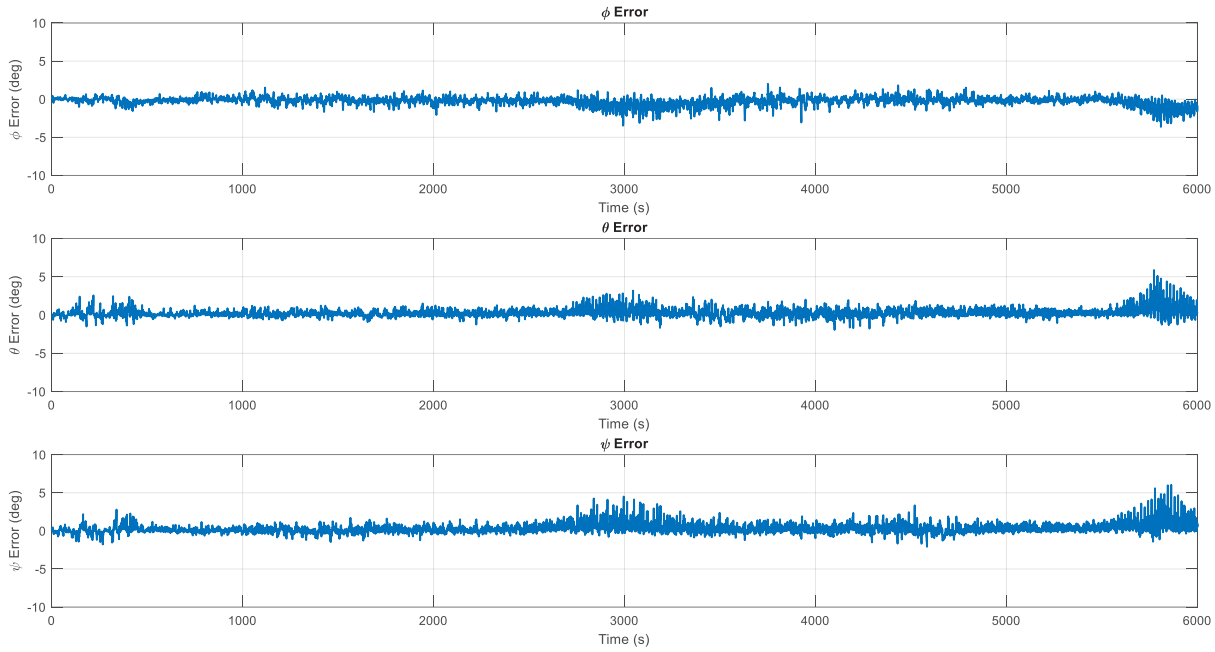

Fig. 7. Euler angles of the attitude determination errors

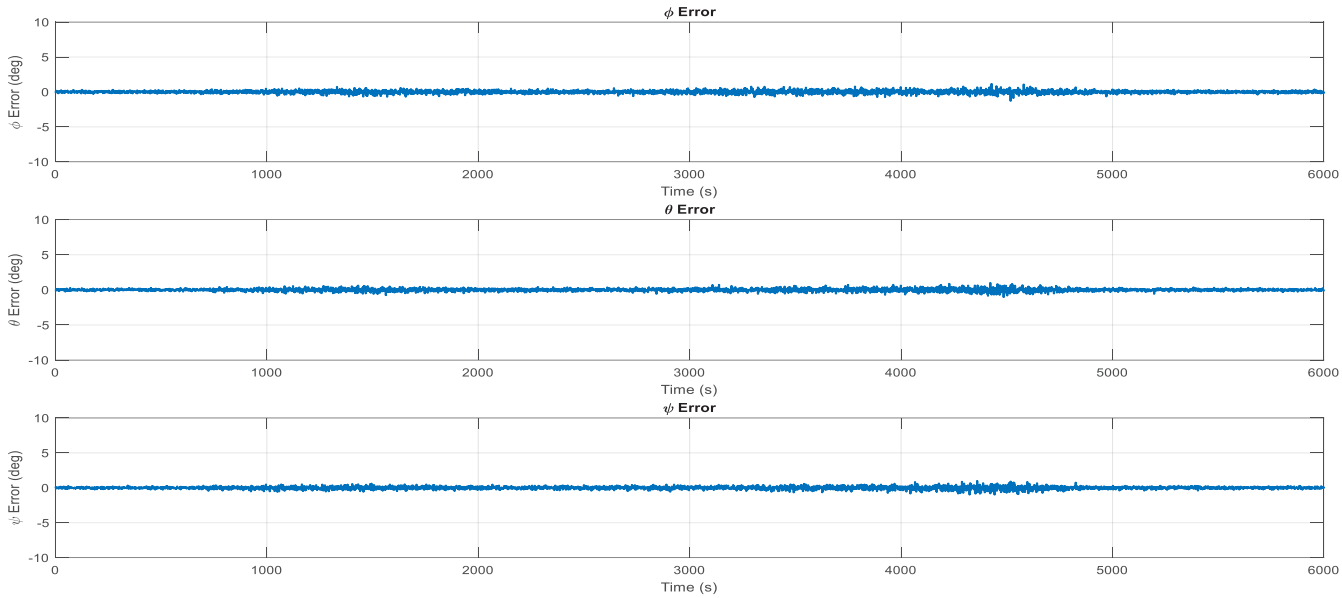

Fig. 8. Euler angles of the attitude determination errors by using EKF and data fusion

6- Conclusions

In this research, a new generation of sensors for the spacecraft attitude determination process is presented. This approach could improve and solve some problems with this task, such as attitude determination in eclipse. This sensor measures the vector's components of the externally imposed electric field in three axes of a satellite's body frame by using three nonlinear capacitors. The capacitors are actuated by sinusoidal voltage and analytically prove that the induced external electric field has a straight effect on the second harmonic of the RC circuits' current signal. By measuring the second harmonic amplitude of each circuit current signal and calibrating them, we can measure the components of the induced electric field and use the vector in the attitude determination algorithm. Considering the effects of the imposed electric field on capacitors, the current of the circuit signal is simulated to justify this theory. Afterwards, by Fast Fourier Transform (FFT) of the circuit current signal, the second harmonic amplitude, the relation between the magnitudes of the induced electric field components and the second harmonic amplitude are investigated. According to figure (2), the maximum second harmonic amplitude occurs in about $V_m = 5volts$. On the other hand, the relation between the analytical results and the simulation studies are confirmed.

Low power consumption, weight, and price and its operation in the whole orbit are the main advantages of this sensor. There are also some disadvantages; for instance, the accuracy of attitude determination by these sensors cannot be so high at the moment, due to some uncertainties in the model of Earth Magnetic Field. This problem can be solved by fusing their data with other sensors' data, and using some filter algorithms. On the other hand, this sensor is only applicable in low altitude orbit. Therefore, the other disadvantage is the limitation of using the sensor in the satellite with high altitude.

Further work can concern optimizing the sensor's parameters such as actuated voltage frequency and amplitude, capacitor's shape and size, and the materials of the dielectric. The mechanical design, manufacturing, test, and calibration also consider after optimization as the future works.

References

[1] Fadly, M., et al. "Deterministic and recursive approach in attitude determination for InnoSAT." Telkomnika 9.3 583 :(2011).

[2] Markley FL and Crassidis JL. Fundamentals of spacecraft attitude determination and control. Springer, 2014.

[3] Wertz JR. Spacecraft attitude determination and control. Springer Science & Business Media, 2012.

[4] Herrera-May AL, Soler-Balcazar JC, Vázquez-Leal H, et al. Recent advances of MEMS resonators for Lorentz force based magnetic field sensors: Design, applications, and challenges. Sensors 2016; 16: 1359.

[5] Li M, Sonmezoglu S, and Horsley DA. Extended bandwidth Lorentz force magnetometer based on quadrature frequency modulation. Journal of Microelectromechanical Systems 2015; 24: 333-342.

[6] Wu G, Xu D, Xiong B, et al. Design, fabrication and characterization of a resonant magnetic field sensor based on mechanically coupled dual-microresonator. Sensors and Actuators A: Physical 2016; 248: 1-5.

[7] Laghi G, Dellea S, Longoni A, et al. Torsional MEMS magnetometer operated off-resonance for in-plane magnetic field detection. Sensors and Actuators A: Physical 2015; 229: 218-226.

[8] Gopal R. Fabrication of MEMS xylophone magnetometer by anodic bonding technique using SOI wafer. Microsystem Technologies 2017; 23: 81-90.

[9] Grosz, Asaf, Michael J. Haji-Sheikh, and Subhas C. Mukhopadhyay, eds. High sensitivity magnetometers. Switzerland: Springer, 2017.

[10] Rezaei, Mohsen, et al. "Attitude determination sensor for low Earth orbit satellite based on Lorentz force." Proceedings of the Institution of Mechanical Engineers, Part G: Journal of Aerospace Engineering 233.6 2230-2219 :(2019).

[11] Damjanovic, Dragan, Paul Muralt, and Nava Setter. "Ferroelectric sensors." IEEE sensors journal :(2001) 1.3 206-191.

[12] Wahba G. A least squares estimate of satellite attitude. SIAM review 1965; 7: 409-409.

[13] Shuster MD and Oh SD. Three-axis attitude determination from vector observations. Journal of Guidance, Control, and Dynamics 1981; 4: 70-77.

[14] Gibbs, Bruce P. Advanced Kalman filtering, least-squares and modeling: a practical handbook. John Wiley & Sons, 2011.

[15] Johnson, Kenneth M. "Variation of dielectric constant with voltage in ferroelectrics and its application to parametric devices." Journal of Applied Physics 33.9 2831-2826 :(1962).

[16] Narayanan, Manoj, et al. "Modified Johnson model for ferroelectric lead lanthanum zirconate titanate at very high fields and below Curie temperature." Applied Physics Letters 022907 :(2012) 100.2.

[17] Cilden-Guler, Demet, Zerefsan Kaymaz, and Chingiz Hajiyev. "Geomagnetic disturbance effects on satellite attitude estimation." Acta Astronautica 180 (2021): 701-712.

HOW TO CITE THIS ARTICLE

M. Rezaei, Ka. Raissi, H. Hashemi Mehne, Y. Norouzi, The New Generation of Attitude Determination Sensor for LEO Satellite based on Induced Electric Field, AUT J. Elec. Eng., 54(1) (2022) 29-38.

DOI: 10.22060/eej.2021.18885.5363